J Mater Sci (2007) 42:3613–3620
DOI 10.1007/s10853-006-0400-5

Preparation, characterization, conductivity and thermal expansion studies of $Ca_{0.5}SbMP_3O_{12}$ (M = Al, Fe, Cr)

G. Rambabu · K. Koteswara Rao · N. Anantharamulu · M. Raghavender · G. Prasad · V. Prashanth Kumar · C. Vishnuvardhan Reddy · Muga Vithal

Received: 25 August 2005 / Accepted: 2 May 2006 / Published online: 30 January 2007

Abstract Nasicon type compounds of general formula $Ca_{0.5}SbMP_3O_{12}$ (M = Al, Fe, Cr) are prepared by solid-state method. All the compounds crystallize in hexagonal lattice with $R\bar{3}c$ space group. The IR spectra show characteristic PO_4 vibrations. Conductivity studies indicate the presence of charged defects. The Cole-Cole plots of impedance are semicircles between 150 and 350 °C. The thermal expansion of these samples is studied in the temperature range 25–500 °C.

Introduction

Sodium zirconium silico phosphate ($Na_{1+x}Zr_2P_{3-x}Si_xO_{12}$), more commonly known as NASICON (sodium (Na) super (S) ionic (I) conductor (CON)) and related sodium zirconium phosphate, $NaZr_2P_3O_{12}$ (NZP) have attracted much attention during last two decades [1–4]. The general formula of these complex phosphates is $A_xMM'(PO_4)_3$. The ''A'' site can be occupied by alkali, alkaline earth, Cu^{2+}, Cu^{+}, Ag^{+}, H^{+} or NH_4^{+} ions. The M and M′ sites are occupied by tri-, tetra- and penta-valent ions. The hexagonal structure is characterized by a network formed by corner sharing of PO_4 tetrahedra with $MO_6/M'O_6$ octahedra forming a ribbon along *c*-axis. These ribbons are interconnected by PO_4 tetrahedra along the *a*-axis. This skeletal arrangement gives tunnels/interstitial sites which accommodate ''A'' ions [5, 6]. The structure is flexible for substitution at A, P, M and M′ giving rises to a variety of isostructural compounds. The interest in these types of phosphates arises due to their fast ionic conductivity [1], near zero thermal expansion behaviour [4, 7–10], high-temperature stability, intercalation/deintercalation behaviour and large surface area. Due to these properties they are widely used as solid electrolytes in high-temperature fuel cells, as heat exchangers, mirror blanks for space technology, as ion-selective electrodes, hosts for radioactive waste and as catalyst supports [11–13] Further, this framework structure gives an opportunity to tailor properties such as ionic conductivity, thermal expansion coefficient, ion selectivity and their correlation with structure. In the present study we report the preparation, characterization (powder X-ray data and infra red (IR) data), the ionic conductivity (DC and AC) and thermal expansion studies of $Ca_{0.5}SbAlP_3O_{12}$, $Ca_{0.5}SbCrP_3O_{12}$, $Ca_{0.5}SbFeP_3O_{12}$ (here after CSAP, CSCP, CSFP, respectively).

G. Rambabu · K. Koteswara Rao · N. Anantharamulu · M. Vithal (✉)
Department of Chemistry, Osmania University, Hyderabad 500 007, India
e-mail: muga_vithal@osmania.ac.in

M. Raghavender · G. Prasad · V. P. Kumar · C. V. Reddy
Department of Physics, Osmania University, Hyderabad 500 007, India

Experimental selection

Preparation

The NASICON compounds $Ca_{0.5}SbMP_3O_{12}$ (M = Al, Cr and Fe) are synthesized by conventional solid-state reaction using AR grade chemicals $CaCO_3$, Sb_2O_5,

$NH_4H_2PO_4$ and metal oxides (Al_2O_3, Cr_2O_3 and Fe_2O_3). Cr_2O_3 is obtained by thermal decomposition of $(NH_4)_2Cr_2O_7$. Fe_2O_3 is prepared by calcination of ferrous oxalate dihydrate at 600 °C. Al_2O_3 and Sb_2O_5 are dried at 200 °C and used without further treatment. The calculated amounts of the starting materials for 10 g of desired sample in single batch are thoroughly mixed and ground together with spectral acetone in an agate mortar for 1 h to give homogeneous mixture. The ground mixture is placed in silica crucible and heated slowly in an electrical furnace to 300 °C and kept for 4 h at that temperature to facilitate the decomposition of ammonium dihydrogen orthophosphate. The mixtures are sequentially heated (at the rate of 0.5 °C/min) in silica crucible at 400 (10 h), 500 (10 h), 600 (10 h), 700 (10 h), 800 (24 h) and finally at 900 °C (24 h) with intermediate grindings after each heat treatment. The reason for following such a sequence of heat treatment is to avoid the formation of pyrophosphate byproduct ($Ca_{0.5}MP_2O_7$ with M = Cr, Fe) along with un-reacted metal oxide impurities.

X-ray powder diffraction

Powder X-ray diffractograms are recorded at room temperature on Philips X'pert Analytical X-ray diffractometer using Nickel filtered Cu-Kα radiation of wavelength 1.5406 Å. The scan rate is 3°/min in the range 2θ = 10–70°. The unit cell parameters are calculated using the least square fitting. Experimental densities of sintered pellets are measured by Archimedes principle using xylene as immersion liquid. Calculated densities are obtained from unit cell dimensions.

Infra red spectra

Infrared spectra are recorded in the form of KBr pellets in the wave number range 4,000–500 cm^{-1} using JASCO FT/IR-5300 Spectrometer.

Ionic conductivity and impedance measurements

Cylindrical pellets (≈10 mm diameter and ≈4 mm thickness) of the samples are obtained by applying uniaxial pressure of 200 MPa. The pellets are sintering at 800 °C for 24 h. The DC conductivities in the temperature range 300–623 K are measured using a two-probe method on the sintered pellets coated with silver paint. A conventional sample holder and Kiethley Electrometer 610C are used. The bulk DC conductivity of all the samples is calculated by measuring the bulk resistance and the sample dimensions. The bulk resistance of the samples is obtained by measuring the current at constant applied voltage of 1.6 V connected in series with Kiethley Electrometer and the sample.

AC Impedance measurements are carried out using HP4192A Impedance analyser from room temperature to 350 °C in the frequency range 100 Hz–1 MHz. The data acquisition is automated by interfacing the instruments (both DC conductivity and impedance measurements) with a personal computer.

Thermal expansion measurements

The relative thermal expansions of the samples are measured using NETZSCH 402 PC dilatometer in air in the temperature range 25–500 °C. The samples are pressed into rectangular rods of size 25 mm × 6 mm × 6 mm for these measurements. The heating and cooling rates are 5°/min.

Results and discussion

Powder X-ray diffraction data

The room temperature powder X-ray diffractograms of all the three compounds are shown in Fig. 1. The peaks observed in XRD are indexed assuming a rhombohedral structure. Since no extra peaks are observed, it may be concluded that there are no detectable impurities or unreacted reactants. These XRD patterns are isomorphous to that of lithium, sodium and calcium containing nasicon frameworks reported earlier [5, 6, 14]. Using the observed d-lines, the unit cell parameters are derived by least-square fit program. All the compositions

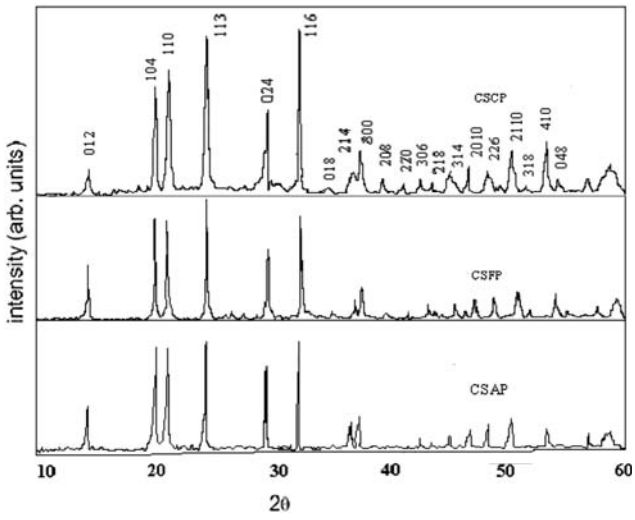

Fig. 1 XRD patterns for $Ca_{0.5}SbMP_3O_{12}$ (M = Al, Cr and Fe)

Table 1 Composition, lattice parameters and densities of $Ca_{0.5}M^{V}M^{III}P_3O_{12}$

Compound	Lattice parameters		Observed density (g/cm^3)	Calculated density (g/cm^3)	Reference
	a (Å)	c (Å)			
$Ca_{0.5}SbAlP_3O_{12}$	8.56	21.87	4.123	4.128	This work
$Ca_{0.5}SbCrP_3O_{12}$	8.61	22.08	4.238	4.321	This work
$Ca_{0.5}SbFeP_3O_{12}$	8.64	21.95	4.272	4.302	This work
$Ca_{0.5}NbAlP_3O_{12}$	8.55	21.88	4.074	4.05	[14]
$Ca_{0.5}NbGalP_3O_{12}$	8.59	22.01	4.415	4.42	[14]
$Ca_{0.5}NbFeP_3O_{12}$	8.6	21.91	4.294	4.28	[14]
$Ca_{0.5}NbInP_3O_{12}$	8.7	22.45	4.627	4.6	[14]

prepared in the present study crystallize in rhombohedral lattice with space group $R\bar{3}c$. A small variation in the lattice parameters is observed which may be attributed to the variation of the size of trivalent metal ion. Using the lattice parameters, Avogadro's number and mass of the sample theoretical (X-ray) densities are calculated. The theoretical and experimental densities agree well within the experimental error. Hence the porosity of the samples is small indicating the well-sintered nature of the pellets. The lattice parameters obtained for all the compounds and densities are presented in Table 1, along with the lattice parameters and densities of other similar calcium nasicon compositions for a comparison.

IR data

The IR spectra of $Ca_{0.5}SbMP_3O_{12}$ (M = Al, Cr and Fe) in the range 1,500–400 cm^{-1} are shown in Fig. 2. All the compounds exhibit strong absorptions below 1,500 cm^{-1}. Generally the vibrational modes of nasicon phases can be due to PO_4 tetrahedra (internal and external modes) and to lattice modes of metal octahedra. The bands corresponding to PO_4 unit are more prominent than that of metal octahedra. The assignments for the observed bands have been made based on the predictions of factor group analysis [15–17]. The PO_4 tetrahedra give nine vibrational modes: (i) the symmetric PO stretching (ν_s or ν_1), (ii) antisymmetric PO stretching (ν_d or ν_2), (iii) symmetric OPO bending (δ_d or ν_3) and (iv) antisymmetric harmonic OPO bending (δ_d or ν_4) [18]. Among these vibrations, both ν_3 and ν_4 are triply degenerate, ν_2 is doubly degenerate and ν_1 is non-degenerate. The asymmetric and harmonic bending vibrations (ν_4) are found in the range 545–680 cm^{-1} while the symmetric PO vibrations (ν_1) are observed in the narrow range 1,020–1,030 cm^{-1}. The symmetric OPO bending vibrations (ν_3) for are seen in the range 1,100–1,160 cm^{-1} and asymmetric PO stretching (ν_2) occurs at 440–450 cm^{-1} in the present samples (Table 2). The absence of any IR bands in the region 740–720 cm^{-1} indicates the absence of pyro phosphate ($P_2O_7^{4-}$) impurity [13]. Similar types of spectra are obtained for silver, sodium and lithium analogues [19, 20].

DC conductivity

Figure 3 shows the variation of DC conductivity with temperature for all the samples. The conductivity ($\log(\sigma T)$) values vary by more than ten orders in the temperature range of present measurements. At high temperatures the samples have high conductivities; however a two-probe method of measurement is used for entire temperature range of conductivity measurements. The DC conductivity is a temperature-activated property and is found to obey the Arrhenius dependence given by

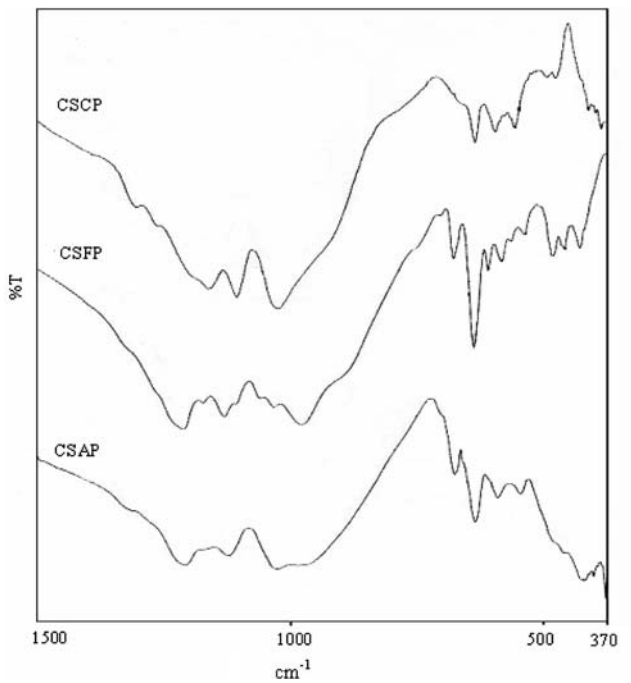

Fig. 2 IR patterns for $Ca_{0.5}SbMP_3O_{12}$ (M = Al, Cr and Fe)

Table 2 IR data $Ca_{0.5}SbMP_3O_{12}$ (M = Al, Cr and Fe)

Compound	O–P–O asymmetric bending vibration (ν_4)	O–P–O harmonic bending vibration (ν_4)	P–O–P stretching vibration	$(PO4)^{3-}$ ionic group vibration (ν_1)	$(P–O)^{(-)}$ ionic vibration (ν_3)
$Ca_{0.5}SbAlP_3O_{12}$	545, 591	636, 677	–	1,029	1,125
$Ca_{0.5}SbCrP_3O_{12}$	546, 585	627	–	1,024	1,104, 1,159
$Ca_{0.5}SbFeP_3O_{12}$	539, 582	636, 679	–	1,029	1,128

The band positions and assignments are in cm^{-1}

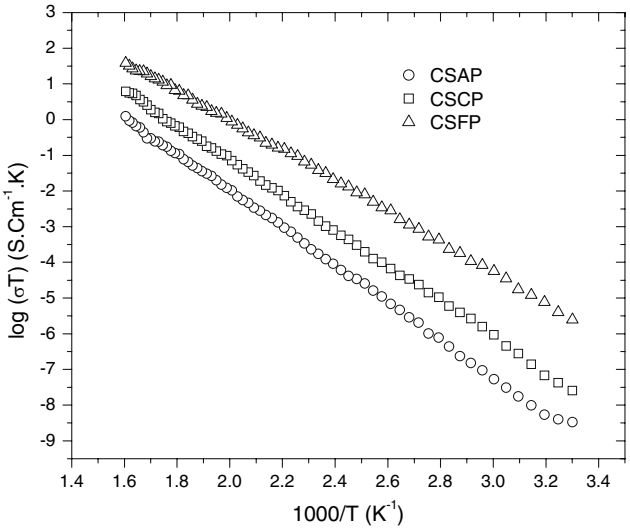

Fig. 3 Arrhenius plots of DC conductivity

$$\sigma_{DC}T = \sigma_0 \exp(-E_a/kT) \quad (1)$$

where σ_0 is the conductivity at infinite temperature, T is the absolute temperature, E_a is the activation energy for conduction and k is the Boltzmann's constant. The activation energies are calculated from the slopes of the plots and are listed in Table 3. It is observed that the conductivity increased around three to four orders in magnitude, from 150 to 350 °C. The activation energies of conduction are found to be in the range 0.84–1.03 eV. These values are slightly higher than the activation energies observed for silver nasicons [19]. Among the three systems investigated, it is noticed that the conductivity is highest at 350 °C (6.21×10^{-2} Ohm^{-1} cm^{-1}) for CSFP sample. It is interesting to observe that the activation energy of conduction and the conductivity values at 350 °C are related inversely. It is also observed that the conductivity at a given temperature follow the order CSFP > CSCP > CSAP.

Impedance study

Impedance spectra of all the materials were studied in the temperature range 30–350 °C and in the frequency range 10^2 to 10^6 Hz. Figure 4(a, b, c) shows complex impedance plots for CSAP, CSCP and CSFP samples respectively at temperatures 300 and 350 °C. Semicircle behaviour of complex impedance is observed for all the samples above 150 °C. However, a complete single semicircle is observed at temperatures 250, 300 and 350 °C. All these plots terminate at the origin indicating the absence of series resistance in the equivalent circuit model of the sample. All the semicircles start on the real impedance axis at the lowest frequency. This starting point is found to decrease with increase in the temperature. This behaviour of complex impedance plots is characteristic of conducting nature of the samples and hence it may be concluded that there is no series capacitance in the equivalent circuit representation of the sample. The radius of the semicircles is decreasing with increase of temperature. Low-frequency intercepts of these semicircles on real axis give the bulk resistance of the sample at the temperature of the complex impedance plots. The absence of second semicircle at lower frequencies indicates the absence of

Table 3 The DC conductivities of all compounds at 150 and 350 °C with activation energy of conduction (E_a DC)

Compound	From DC conductivity			From AC impedance		
	σ_{DC} at 150 °C (ohm^{-1} cm^{-1})	σ_{DC} at 350 °C (ohm^{-1} cm^{-1})	E_a DC (eV)	$\sigma(0)$ at 150 °C (ohm^{-1} cm^{-1})	E_a(bulk) (eV)	E_a(relax) (eV)
$Ca_{0.5}SbAlP_3O_{12}$	2.91×10^{-7}	1.99×10^{-3}	1.028	1.27×10^{-9}	0.961	1.074
$Ca_{0.5}SbCrlP_3O_{12}$	2.27×10^{-6}	9.82×10^{-3}	0.977	1.28×10^{-10}	1.088	1.108
$Ca_{0.5}SbFeP_3O_{12}$	7.42×10^{-6}	6.21×10^{-2}	0.839	8.08×10^{-9}	0.915	1.031

The $\sigma(0)$ (at 150 °C) obtained by fitting the AC conductivity data to Eq. 3 and the activation energies for bulk conductivity and dielectric relaxation

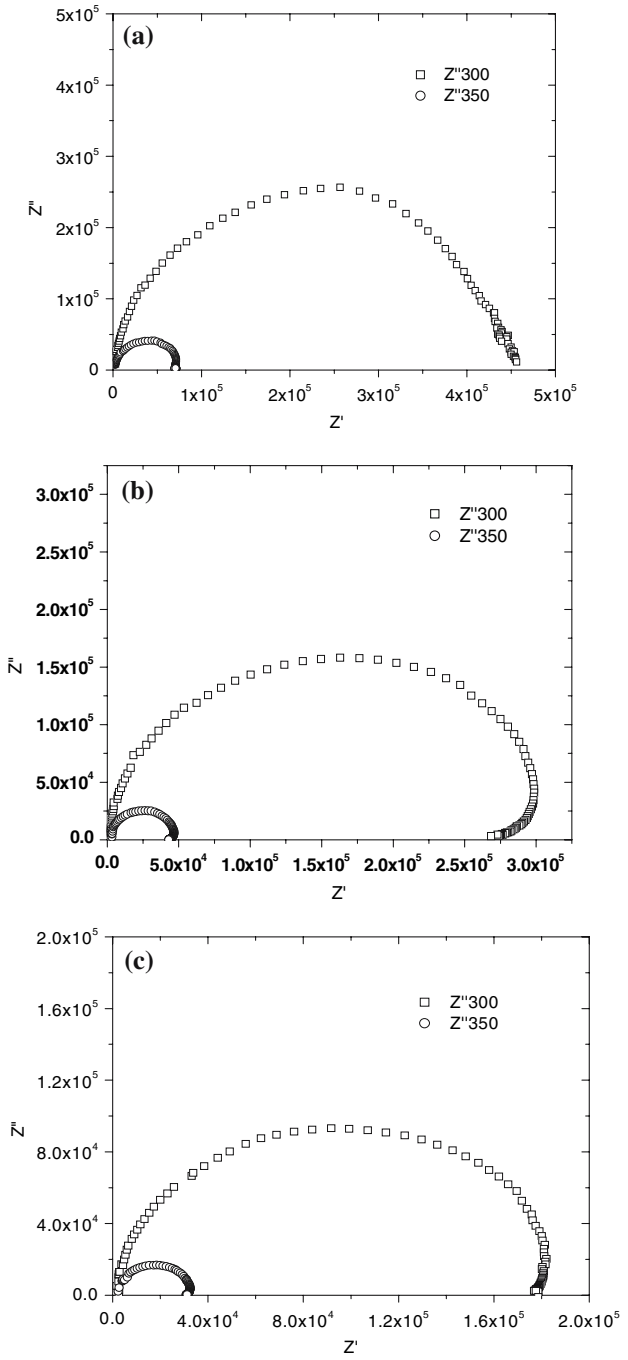

Fig. 4 Complex impedance plots of (**a**) CSAP, (**b**) CSCP and (**c**) CSFP at 300 and 350 °C

observable grain boundary resistance and electrode effects [21].

The bulk resistances, together with the sample dimensions are used to determine the bulk conductivity (grain conductivity) of all these samples. The variation of bulk conductivity with inverse of temperature is plotted on semi-log scale and shown in Fig. 5. We found that the activation energy of CSFP is lower than other two samples (CSAP and CSCP).

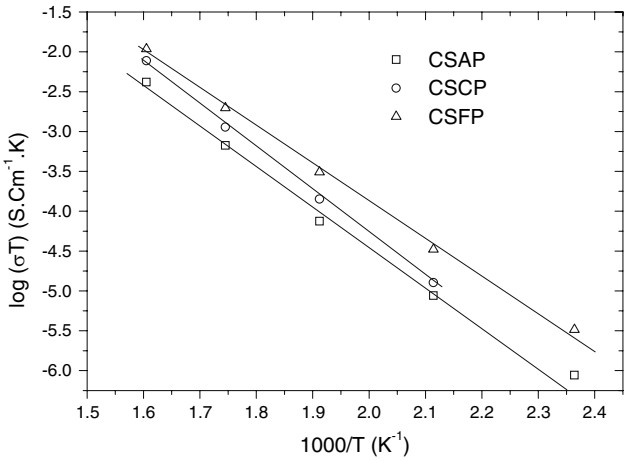

Fig. 5 Conductivity obtained from low-frequency intercept of complex impedance plots versus inverse of temperature

The activation energies estimated from DC conductivity and AC conductivity of lowest frequency obtained from complex impedance plots are comparable with each other (Table 3).

To confirm whether the overall sample resistance represents the bulk resistance of the grains or being influenced by grain boundary effects, the experimental data are replotted as the imaginary parts of the impedance, Z'' and electric modules, M'' against log frequency and is shown in Fig. 6 for the all three samples at 250 °C. The data for all samples shows single peaks in both Z'' and M'' spectra, separated in frequency by about half a decade. The peaks are somewhat broader than an ideal Debye peak. The peak width at half maxima is of ~1.32 decades compared to 1.14 decades for Debye peak [19, 22]. The height of M'' peak at various temperatures is found to be in the range 0.00235–0.00354. For an ideal Debye solid M'' is given by

$$M'' = \frac{C_0}{2C} \tag{2}$$

Here $C_0 = (\varepsilon_0 A)/d$ (where A and d are area and thickness of the pellet, ε_0 is permittivity of the free space), C is the capacitance of the pellet, which is calculated from the relation, $\omega RC = 1$ ($\omega = 2\pi f_{max}$, R = the resistance obtained at lower frequency on the Cole-Cole plot). The calculated M'' values from the above equation are found to be very close to that of observed values. Since the peaks in Z'' and M'' versus frequency curves are almost coincident and there is no evidence for any additional peaks at lower frequency in the Z'' spectrum, it may be concluded that the observed results represent bulk conductance only [19, 22].

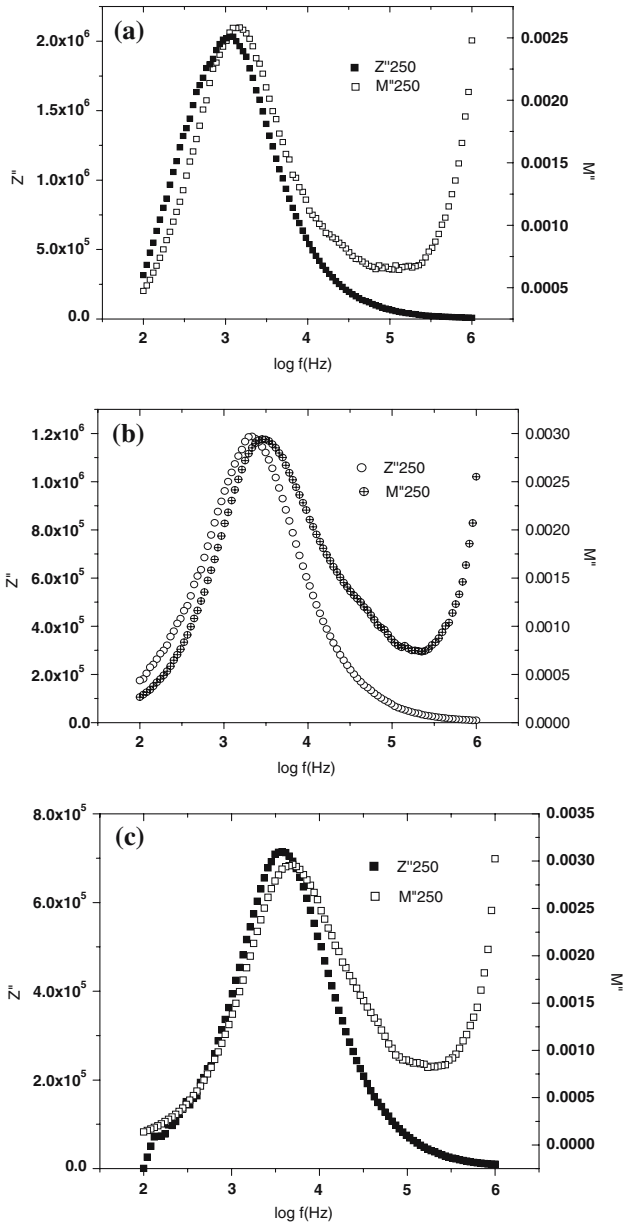

Fig. 6 Plots of log *f* versus *Z″*, *M″* for (**a**) CSAP, (**b**) CSCP and (**c**) CSFP at 250 °C

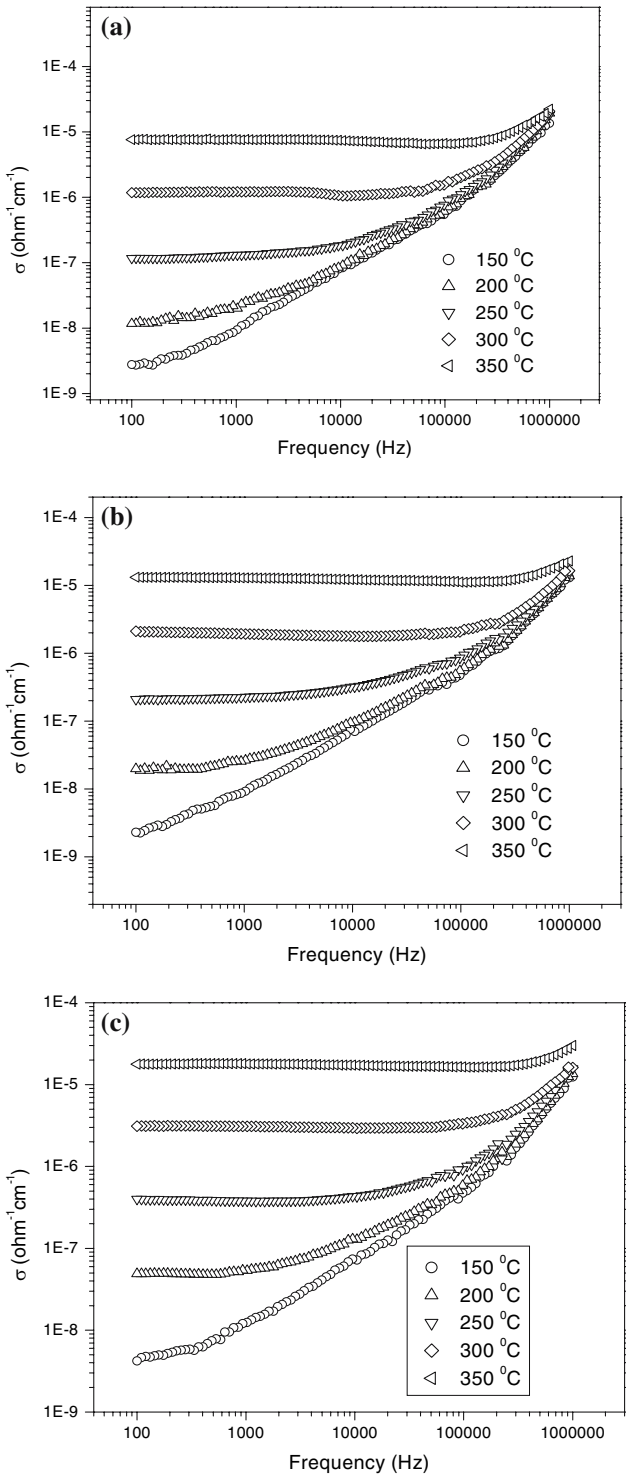

Fig. 7 Frequency variation of AC conductivity for (**a**) CSAP, (**b**) CSCP and (**c**) CSFP at different temperatures

Figure 7(a, b, c) shows the conductivity data in the frequency range 10^2 to 10^6 Hz at different temperatures for all samples. The frequency-dependent conductivity in Fig. 7(a, b, c) have following features:

1. All the three samples show similar frequency-dependent conductivity at different temperatures.
2. The absence of a blocking electrode effect is evidenced from the frequency-independent conductivity (plateau region) at lower frequency for temperature 200 °C and above. However at 150 °C the plot shows an increasing conductivity with increasing frequency.
3. The Plateau region (frequency-independent conductivity) of conductivity increases with increase in temperature and the value of plateau region conductivity also increase with temperature.

Table 4 The best-fit values of n_1, n_2, σ_0, A and B for CSAP (Ref. Eq. 3)

Temp. (K)	n_1	n_2	σ_0	A	B
423	0.72	1.57	1.270×10^{-9}	6.097×10^{-11}	5.288×10^{-12}
473	0.58	1.45	1.120×10^{-8}	5.092×10^{-10}	2.416×10^{-12}
523	0.52	1.41	1.127×10^{-7}	5.191×10^{-10}	6.205×10^{-14}
573	0.54	1.42	1.023×10^{-6}	5.926×10^{-10}	4.142×10^{-10}
623	0.50	1.44	6.997×10^{-6}	5.092×10^{-10}	4.425×10^{-14}

4. At very high frequencies the conductivity is found to be linearly dependent on frequency (increases with increasing frequency).

The AC conductivity data is fit to the following equation:

$$\sigma(\omega) = \sigma_0 + A\omega^{n_1} + B\omega^{n_2} \quad (3)$$

The values of exponents n_1 and n_2 along with σ_0, A and B for CSAP are given in Table 4. The values of n_1 are found to be less than 1 and values of n_2 are greater than 1. With the increase of temperature the values of n_1 and n_2 have decreased. Frequency-dependent nature of the exponents n_1 and n_2 is a measure of the disorder present and the type of charge aggregation in the samples. Frequency and temperature-dependent variation of these parameters indicates the change in the character of the charged defects in the samples with the temperature and frequency. Observation of two distinct slopes in the frequency dependence in conductivity indicates the presence of two different frequency-dependent conductivity mechanisms in the samples. It is observed that CSAP has low conductivity and CSFP has high conductivity among the three compounds. However at high-frequency region the conductivity pattern of all the three samples merge into a single curve.

Dilatometry

Bulk thermal expansion curves of CSAP, CSCP and CSFP samples up to 500 °C are given in Fig. 8. Thermal expansion coefficients (α) is calculated using:

$$\alpha = \frac{l_2 - l_1}{l_1(T_2 - T_1)} \quad (4)$$

where l_1 and l_2 are lengths at temperatures T_1 and T_2 respectively. The α values are tabulated in Table 5 for all the samples along with the some reported values for similar systems.

It is seen from Fig. 8 that all the samples show a near linear thermal expansion behaviour. These samples exhibit positive thermal expansion coefficient and near zero thermal expansion is observed up to ≈70 °C. The thermal expansion observed may be due to bending and distortion of PO_4 tetrahedra and MO_6 octahedra as suggested by Alamo [23]. The thermal expansion

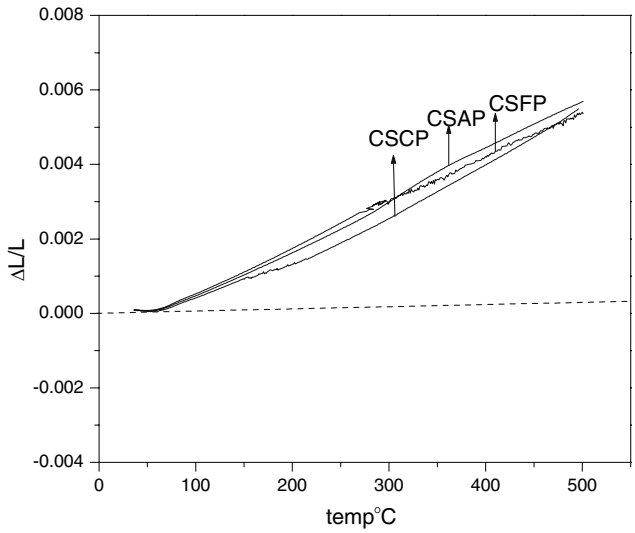

Fig. 8 $\Delta L/L$ versus temperature plots

Table 5 Compositions and coefficients of thermal expansion

S. No.	Composition	$\alpha \times 10^{-6}$/°C (25–500 °C)	Reference
1	$Ca_{0.5}SbAlP_3O_{12}$	4.71	This work
2	$Ca_{0.5}SbCrP_3O_{12}$	2.97	This work
3	$Ca_{0.5}SbFeP_3O_{12}$	4.95	This work
4	$Ca_{0.5}Ti_2P_3O_{12}$	5.10	[7]
5	$Ca_{0.5}Zr_2P_3O_{12}$	–1.60	[7]
6	$NaTi_2P_3O_{12}$	–5.50	[7]
7	$Na_3Cr_2P_3O_{12}$	5.30	[7]
8	$Na_{3/2}Zr_{15/8}P_3O_{12}$	–2.35	[7]
9	$Ca_{0.25}Na_{0.5}Zr_2P_3O_{12}$	6.30	[7]
10	$Ca_{0.25}Na_{0.5}Ti_2P_3O_{12}$	4.00	[7]
11	$Na_{1.5}Zr_{1.5}Cr_{0.5}P_3O_{12}$	0.50	[7]
12	$LiZr_2P_3O_{12}$	9.70	[8]
13	$NaZr_2P_3O_{12}$	–3.00	[8]
14	$KZr_2P_3O_{12}$	–7.50	[8]
15	$RbZr_2P_3O_{12}$	–1.50	[8]
16	$CsZr_2P_3O_{12}$	–0.50	[8]
17	$Mg_{0.5}Zr_2P_3O_{12}$	2.11	[10]
18	$Ca_{0.5}Zr_2P_3O_{12}$	–2.11	[10]
19	$Sr_{0.5}Zr_2P_3O_{12}$	3.16	[10]
20	$Ba_{0.5}Zr_2P_3O_{12}$	3.37	[10]

coefficients of CSAP and CSFP are 4.8×10^{-6} and 4.9×10^{-6}/°C, respectively which are nearly equal. This may be due to near equal ionic sizes of Al^{3+} (5.4 nm) and Fe^{3+} (5.5 nm). The thermal expansion coefficient of CSCP is 2.9×10^{-6}/°C , which is lower than the other two samples value. The ionic size of Cr^{3+} (6.2 nm) is slightly higher than Al^{3+} and Fe^{3+}. This may lead to relatively less distortion in PO_4 tetrahedra and MO_6 octahedra in CSCP sample leading to observation of lower thermal expansion coefficient. However, a detailed high-temperature X-ray studies are necessary to confirm this conclusion.

Conclusion

In conclusion, $Ca_{0.5}SbMP_3O_{12}$ (M = Al, Fe, Cr) samples prepared show interesting electrical and thermal expansion behaviour. The electrical studies indicate the existence of electrically charged defects, which are relaxing. The activation energies for conduction and relaxation show interesting variation with the change of ionic radius of M ions. The tetrahedral and octahedral distortions may be responsible for observed changes in thermal expansion.

Acknowledgements The authors would like to thank Head, Department of Physics, Osmania University for extending powder XRD facility. The authors wish to thank Dr. J.A.R.P. Sarma for fruitful discussions. One of us (K.K.R) thanks CSIR, New Delhi for financial assistance.

References

1. Goodenough JB, Hong HYP, Kafalas JA (1976) Mater Res Bull 11:303
2. Hong HY-P (1976) Mater Res Bull 11:173
3. Alamo J, Roy R (1984) J Am Ceram Soc 67:C78
4. Roy R, Agarwal DK, Roy RA (1984) Mater Res Bull 19:471
5. Hagman LO, Kierkegaard P (1968) Acta Chem Scand 22:1822
6. Sljukic M, Matkovic B, Prodic B (1969) Ziet Kistal 130:148
7. Agarwal DK, Stubican VS (1985) Mater Res Bull 20:99
8. Lenain GE, McKinstry HA, Limaye SY, Woodword A (1984) Mater Res Bull 19:1451
9. Oota T, Yamai I (1986) J Am Ceram Soc 69:1
10. Limaye SY, Agarwal DK, McKinstry HA (1987) J Am Ceram Soc 70:C232
11. Roy R, Vance ER, Alamo J (1982) Mater Res Bull 17:585
12. Agarwal DK, Adair JH (1990) J Am Chem Soc 71:2153
13. Brik Y, Kachimi M, Verduraz FB, Ziyad M (2001) Microporous Mesoporous Mater 43:103
14. Srinivasulu B, Vithal M (1999) J Mater Sci Lett 18:1771
15. Barj M, Perthius H, Colombon Ph (1983) Solid State Ionics 11:157
16. Mbandza A, Bordes E, Courtine P (1985) Mater Res Bull 20:251
17. Barg M, Lucazeau G, Delmas C (1992) J Solid State Chem 100:141
18. Le Polles G, Videau JJ, Olazcuaga R, Couzi M (1996) J Solid State Chem 127:341
19. Koteswara Rao K, Rambabu G, Raghavender M, Prasad G, Kumar GS, Vithal M (2005) Solid State Ionics 176:2701
20. Kasturi Rangan K, Gopalakrishnan J (1995) Inorg Chem 34:969
21. Jonscher AK (1980) Phys Thin Films 11:232
22. Losilla ER, Aranda MAG, Bruque S, Paris MA, Sanz J, West AR (1998) Chem Mater 10:665
23. Alamo J (1993) Solid State Ionics 63–65:547